

Dynamics of quasiperiodically driven spin systemsSayak Ray¹, Subhasis Sinha² and Diptiman Sen³¹*Department of Chemistry, Ben-Gurion University of the Negev, Beer-Sheva 84105, Israel*²*Indian Institute of Science Education and Research-Kolkata, Mohanpur, Nadia 741246, India*³*Centre for High Energy Physics, Indian Institute of Science, Bengaluru 560012, India* (Received 26 July 2019; revised manuscript received 29 August 2019; published 21 November 2019)

We study the stroboscopic dynamics of a spin- S object subjected to δ -function kicks in the transverse magnetic field which is generated following the Fibonacci sequence. The corresponding classical Hamiltonian map is constructed in the large spin limit, $S \rightarrow \infty$. On evolving such a map for large kicking strength and time period, the phase space appears to be chaotic; interestingly, however, the geodesic distance increases linearly with the stroboscopic time implying that the Lyapunov exponent is zero. We derive the Sutherland invariant for the underlying $SO(3)$ matrix governing the dynamics of classical spin variables and study the orbits for weak kicking strength. For the quantum dynamics, we observe that although the phase coherence of a state is retained throughout the time evolution, the fluctuations in the mean values of the spin operators exhibit fractality which is also present in the Floquet eigenstates. Interestingly, the presence of an interaction with another spin results in an ergodic dynamics leading to infinite temperature thermalization.

DOI: [10.1103/PhysRevE.100.052129](https://doi.org/10.1103/PhysRevE.100.052129)**I. INTRODUCTION**

In recent years quasiperiodic systems have attracted a lot of interest in various contexts ranging from quasicrystals [1–5] to localization-delocalization transitions [6–10], multifractality [11–14], topological phases [15], and so on. The creation of a quasiperiodic potential in one dimension using bichromatic optical lattices [6] has led to the realization of the well-known Aubry-André model [16], which has been studied extensively both theoretically [7,8] and experimentally [9,10,17], in the context of observing localization phenomena, particularly many-body localization in interacting systems [18,19]. In the presence of a periodic drive such many-body localized states exhibit drive-induced delocalization and thermalization of isolated interacting quantum systems [20–22], and its connection with the underlying chaotic dynamics and random matrix theory has been explored [23]. As an extension, several interesting questions can be addressed related to the dynamical behavior of quantum systems under a quasiperiodic drive. One such issue is the emergence of steady states in quasiperiodically driven interacting quantum systems [24,25] and most interestingly, its connection with spectral properties and random matrix theory which is related to ergodicity.

One way to generate a quasiperiodic drive is by perturbing the system under consideration following the Fibonacci sequence; such a sequence has a rich mathematical structure giving rise to an invariant of the corresponding dynamical systems [26–28]. This way of generating a quasiperiodic drive can provide an alternate way to study the quasiperiodic structures observed in Fibonacci lattices [27–29]. The Fibonacci drive can also be generated for a series of incommensurate frequencies known as metallic means, a common example of which is the golden ratio, $\beta_G = (\sqrt{5} + 1)/2$. These driving protocols can give rise to the realization of a strange nonchaotic attractor [30] leading to a fractal-like dynamics

which has been theoretically studied for dynamical maps with quasiperiodicity [31–33] as well observed experimentally [34]. The evolution of a spin-1/2 system under quasiperiodic perturbation reveals various interesting dynamical behaviors and temporal correlations [35–38]. A quasiperiodic drive can also lead to slow relaxation to nonequilibrium steady states which has been investigated for interacting spin systems in the presence of a disordered magnetic field [39]. However, what remains unexplored in all these studies is the properties of the time evolution operator, which naturally raises the following important questions. Under a quasiperiodic drive, is there any underlying fractality in the eigenmodes of the time evolution operator itself, even for noninteracting systems? If so, then what is the fate of such critical states in the presence of interactions and how is it reflected in the dynamics? Recently the study of multifractal eigenstates in models with random or quasiperiodic disorder near metal-insulator transitions both in the presence and absence of interactions has attracted significant attention due to its connection with nonergodicity and anomalous thermalization [40–42]. Multifractality of eigenstates is also exhibited near quantum phase transitions in Ising-like spin models [43], near Mott insulator to superfluid phase transitions in the Bose-Hubbard model [44], and in Luttinger liquids [45]. Interestingly, such multifractal electronic states has recently been observed experimentally near the metal-insulator transition [46]. In this paper we address these issues by considering a simple model of a large spin in the presence of a quasiperiodic drive which allows us to study the classical dynamics in an appropriate limit, at the same time retaining the full information of the time evolution operator. Such a large spin system offers the possibility of studying fractal dynamics at the classical level as well its signature in the eigenstates and spectrum of the corresponding quantum system. Moreover, a generalization of this simple model to two interacting spins provides a way to observe the

change in dynamics to ergodicity due to the interplay between a quasiperiodic drive and interactions.

We first consider a simple model of a noninteracting spin of magnitude S (which has a well-defined classical limit) subjected to a quasiperiodic drive. Our objective is twofold. First, we want to study the dynamics of the corresponding classical system and analyze the fluctuations around the mean values of the spin components. Second, we want to study the quantum dynamics and spectral properties of the time evolution operator, particularly its change in the presence of interaction. The paper is organized as follows. In Sec. II we describe the time-dependent Hamiltonian and the details of the quasiperiodic driving protocol. We then study the dynamics of the corresponding classical system by suitably taking the limit $S \rightarrow \infty$ in Sec. II A. This is followed by the derivation of an invariant for this dynamical system in Sec. II B. The quantum dynamics of a finite spin S and the spectral properties of the time evolution operator are discussed in Sec. II C. The effects of interaction are studied in Sec. III. Finally, we summarize our results, discuss possible experiments which can test our results, and conclude in Sec. IV.

II. DRIVEN SPIN MODEL IN TRANSVERSE MAGNETIC FIELD

The dynamics of a spin- S particle in the presence of a time-dependent magnetic field can be described by the Hamiltonian

$$\hat{H}(t) = \omega_0 \hat{S}_z + \lambda \hat{S}_x \sum_{n=-\infty}^{\infty} \delta\left(t - \sum_n T_n\right), \quad (1)$$

where the first term in the Hamiltonian represents the effect of a magnetic field with strength ω_0 applied along the \hat{z} direction (we have absorbed the gyromagnetic ratio in the definition of ω_0), and the second term represents a δ -function kick due to a transverse magnetic field in the \hat{x} direction with strength λ . Here $\hat{S}_{x,y,z}$'s denote the spin angular-momentum operators and T_n is the time lapse between the $(n-1)$ th and n th kicks. Here we consider the case $T_n = T_0(1 \pm \epsilon) \equiv T_{\pm}$, i.e., the time lapse can take two values T_+ or T_- which follows the Fibonacci sequence:

$$T_+, T_-, T_+, T_+, T_-, T_+, T_-, T_+, \dots \quad (2)$$

We will scale the energy (time) by ω_0 ($1/\omega_0$) and set $\hbar = 1$ throughout this paper.

The time evolution operator describing the dynamics of such system between the $(n-1)$ th and n th kicks is given by

$$\hat{\mathcal{F}}_n = e^{-iT_n \hat{S}_z} e^{-i\lambda \hat{S}_x}. \quad (3)$$

Note that for a periodic drive in which all the T_n 's are equal, Eq. (3) reduces to the usual Floquet operator. Following the time evolution of any operator between the $(n-1)$ th and n th kicks under the Floquet matrix $\hat{\mathcal{F}}_n$ (namely, $\hat{A}_{n+1} = \hat{\mathcal{F}}_n^\dagger \hat{A}_n \hat{\mathcal{F}}_n$) [47], we obtain the Heisenberg equations of motion for the spin operators as follows:

$$\begin{aligned} \hat{S}_x^{n+1} &= \hat{S}_x^n \cos T_n - \sin T_n (\hat{S}_y^n \cos \lambda - \hat{S}_z^n \sin \lambda), \\ \hat{S}_y^{n+1} &= \hat{S}_x^n \sin T_n + \cos T_n (\hat{S}_y^n \cos \lambda - \hat{S}_z^n \sin \lambda), \\ \hat{S}_z^{n+1} &= \hat{S}_y^n \sin \lambda + \hat{S}_z^n \cos \lambda. \end{aligned} \quad (4)$$

This is a linear map for the spin operators of the form: $(\hat{S}_x^{n+1}, \hat{S}_y^{n+1}, \hat{S}_z^{n+1}) = J_n (\hat{S}_x^n, \hat{S}_y^n, \hat{S}_z^n)$, where the transfer matrix J_n can be written as

$$J_n = \begin{pmatrix} \cos T_n & -\sin T_n \cos \lambda & \sin T_n \sin \lambda \\ \sin T_n & \cos T_n \cos \lambda & -\cos T_n \sin \lambda \\ 0 & \sin \lambda & \cos \lambda \end{pmatrix}, \quad (5)$$

where the T_n 's are given in Eq. (2). We will consider the case $\epsilon = 1$, so that Eq. (3) becomes

$$\hat{\mathcal{F}}_1 = e^{-i\lambda \hat{S}_x}, \quad \hat{\mathcal{F}}_2 = e^{-i2T_0 \hat{S}_z} e^{-i\lambda \hat{S}_x}, \quad (6)$$

where $\hat{\mathcal{F}}_1$ represents kicking the spin- S object by a magnetic field in the \hat{x} direction and $\hat{\mathcal{F}}_2$ corresponds to time evolution of the system under \hat{S}_z for time interval $2T_0$ followed by another kick in \hat{S}_x .

Starting from two such $SU(N)$ matrices, $\hat{\mathcal{F}}_1$ and $\hat{\mathcal{F}}_2$, the successive Floquet operators in a Fibonacci sequence can be generated using the recursion relation,

$$\hat{\mathcal{F}}_{m+2} = \hat{\mathcal{F}}_{m+1} \hat{\mathcal{F}}_m, \quad (7)$$

where the initial matrices $\hat{\mathcal{F}}_1$ and $\hat{\mathcal{F}}_2$ are given in Eq. (6). We would like to point out that at a Fibonacci time step m , the stroboscopic time is given by $n = F_m$, where F_m is the m th Fibonacci number. For large m , the stroboscopic time increases exponentially as $n \sim e^{\beta_G m}$, where $\beta_G = (\sqrt{5} + 1)/2$ is the golden ratio. The advantage of using such a recursion relation is that one can numerically obtain the steady state of the system after a very long timescale. Henceforth, we will adopt Eq. (7) to study the dynamics for a very large duration in stroboscopic time.

A. Classical dynamics

We will first discuss the dynamics of the corresponding classical system. The classical limit of such a spin system can be obtained by considering the large spin limit, $S \rightarrow \infty$. Then the spin variables $\hat{S}_{x,y,z}$ can be classically described by the components of a spin vector $\vec{S} \equiv (S_x, S_y, S_z)$. We scale the spin operators by the magnitude S to obtain the classical spin variables, $s_i = S_i/S$ which follow the commutation relations $[s_i, s_j] = i\epsilon_{ijk} s_k/S$. In the limit $S \rightarrow \infty$, the commutators vanish and the variables become classical. Thus using Eqs. (4), the stroboscopic time evolution of the corresponding classical spin variables in between consecutive kicks can be described by the following linear Hamiltonian map:

$$\begin{pmatrix} s_x^{n+1} \\ s_y^{n+1} \\ s_z^{n+1} \end{pmatrix} = J_n \begin{pmatrix} s_x^n \\ s_y^n \\ s_z^n \end{pmatrix}, \quad (8)$$

where the transfer matrix J_n is given in Eq. (5). By evolving Eq. (8) stroboscopically in time we obtain the trajectories on a unit sphere as shown in Fig. 1 for different driving parameters. We observe that for a small driving strength λ and time period T_0 the trajectories are regular and precess over time as depicted in Fig. 1(a). Over a small timescale a similar regular trajectory is plotted in the projected plane of s_x - s_y in Fig. 2(a). However, for large values of λ and T_0 , the dynamics is no longer regular and eventually covers the whole

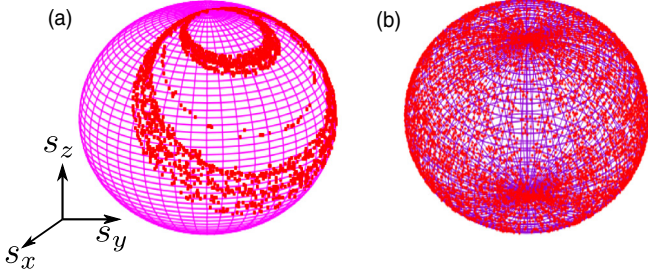


FIG. 1. Stroboscopic dynamics of the spin variables s_x , s_y , and s_z on a unit sphere up to Fibonacci step $m \sim 1000$ for (a) $\lambda = \pi/100$, $T_0 = \pi/50$ and (b) $\lambda = \pi/10$, $T_0 = \pi/10$.

surface of the sphere shown in Fig. 1(b). We note that the transfer matrix in Eq. (5) has determinant equal to 1 and its eigenvalues have the form 1 and $e^{\pm i\varepsilon}$, ε being the eigenphase. As a result, the Lyapunov exponent always turns out to be zero [48–50]. To further illustrate this, we compute the growth of the geodesic distance on the Bloch sphere. We start from the initial point $s_i = (s_x, s_y, s_z) = (0, 0, 1)$ and evolve it under successive kicks following Fibonacci sequence. The resulting trajectory for small λ and T_0 is depicted in the s_x - s_y plane in Fig. 2(a). The geodesic distance between the initial point s_i and the time-evolved point s_f is given by $d = \cos^{-1}(\vec{s}_i \cdot \vec{s}_f)$. In Fig. 2(b) we have plotted d as a function of the stroboscopic time (number of kicks) n ; a linear growth is observed implying that the Lyapunov exponent is zero. The slope of d with n increases on increasing λ , resulting in completely dispersed trajectories in phase space, an example of which is depicted in Fig. 1(b). The vanishing of the Lyapunov exponent is an indication of nonchaotic dynamics, similarly to strange nonchaotic attractors occurring in this case.

B. Fibonacci sequence of SO(3) matrices and Sutherland invariant

We first discuss the case of SU(2) matrices multiplied according to a Fibonacci sequence for which Sutherland found an invariant; then we will discuss how this invariant generalizes to the case of SO(3) matrices. Starting with two SU(2) matrices U_1 and U_2 , we generate a Fibonacci sequence of matrices defined by the recursion relation $U_{m+2} = U_{m+1}U_m$. Let us parametrize U_m as

$$U_m = e^{i\alpha_m \hat{n}_m \cdot \vec{\sigma}} = \cos \alpha_m \mathbb{I}_2 + i \sin \alpha_m \hat{n}_m \cdot \vec{\sigma}, \quad (9)$$

where $0 \leq \alpha_m \leq \pi$, \hat{n}_m is a unit vector, \mathbb{I}_2 denotes the 2×2 identity matrix, and $\vec{\sigma} = (\sigma_x, \sigma_y, \sigma_z)$ denotes the Pauli matrices. Defining $x_m = \frac{1}{2} \text{tr}(U_m) = \cos \alpha_m$, Sutherland showed that the quantity

$$I_s = x_m^2 + x_{m+1}^2 + x_{m+2}^2 - 2x_m x_{m+1} x_{m+2} - 1 \quad (10)$$

is independent of m [28].

We now consider SO(3) matrices denoted as R_m . Starting with two such matrices R_1 and R_2 , we generate a Fibonacci sequence using the recursion relation

$$R_{m+2} = R_{m+1}R_m. \quad (11)$$

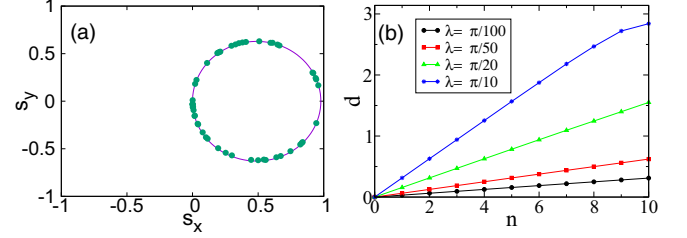


FIG. 2. (a) Dynamics of the spin variables, starting from the initial point $(0,0,1)$, projected onto the s_x - s_y plane for $T_0 = \pi/100$ and $\lambda = \pi/100$, for which $I_s = -2.43 \times 10^{-7} \simeq 0$. The dotted points are obtained numerically by evolving the dynamical map in Eq. (8) up to a few Fibonacci steps $m \sim 50$, and the solid line is drawn using the analytical expression in Eq. (15). (b) Geodesic distance d as a function of the stroboscopic time n for $T_0 = \pi/100$.

Let us parametrize R_m as follows:

$$R_m = e^{i\phi_m \hat{e}_m \cdot \vec{T}}, \quad (12)$$

where $0 \leq \phi_m \leq 2\pi$, \hat{e}_m is a unit vector, and $\vec{T} = (T_x, T_y, T_z)$ are the generators of SO(3) matrices. One can show that the matrix elements of R_m given by R_{ij}^m and the components of \hat{e}_m given by e_i^m are related as

$$R_{ij}^m = \delta_{ij} \cos \phi_m + e_i^m e_j^m (1 - \cos \phi_m) + \sum_{k=1}^3 \epsilon_{ijk} e_k^m \sin \phi_m, \quad (13)$$

where ϵ_{ijk} is the totally antisymmetric matrix with $\epsilon_{123} = 1$. Now using the standard mapping between the spin-1/2 and spin-1 representations of the angular-momentum group, $\alpha_m = \phi_m/2$ and $\hat{n}_m = \hat{e}_m$ one can obtain the Sutherland invariant I_s for a given SO(3) matrix R_m . The analytical expression of the invariant I_s corresponding to the transfer matrices J_m in Eq. (5) is derived in Appendix A. There is a subtlety here: Since the same SO(3) matrix R_m corresponds to two different SU(2) matrices, U_m and $-U_m$, whose traces (divided by 2) are given by x_m and $-x_m$, one has to check at each step of the Fibonacci sequence which of the two possible values of the trace gives the correct value of the Sutherland invariant in Eq. (10).

We will now study what happens when R_m acts on the column $(s_x, s_y, s_z) = (0, 0, 1)$ as numerically shown in Fig. 2(a). Using Eq. (13), we see that

$$\begin{pmatrix} s_x^m \\ s_y^m \\ s_z^m \end{pmatrix} = \begin{bmatrix} e_1 e_3 (1 - \cos \phi_m) - e_2 \sin \phi_m \\ e_2 e_3 (1 - \cos \phi_m) + e_1 \sin \phi_m \\ \cos \phi_m + e_3^2 (1 - \cos \phi_m) \end{bmatrix}. \quad (14)$$

Hence, using the above parametrization for the transfer matrix in Eq. (5), when $\lambda, T_0 \ll 1$, we see that the point (s_x^m, s_y^m) given by

$$(s_x^m, s_y^m) = [e_1 e_3 (1 - \cos \phi_m), e_1 \sin \phi_m], \quad (15)$$

where $e_1 = \lambda/\bar{\lambda}$, $e_3 = 2T_0/\beta_G \bar{\lambda}$, and $\bar{\lambda} = \sqrt{\lambda^2 + 4T_0^2/\beta_G^2}$, describes an ellipse as shown by the solid line in Fig. 2(a) whose center lies at $(e_1 e_3, 0)$ and the lengths of the axes are $2e_1 e_3$ and $2e_1$ in the \hat{x} and \hat{y} directions, respectively (see Appendix A for details).

We mention that quasiperiodic driving of SU(2) matrices has been studied in detail in Refs. [24] and [25]. It has been found that the long-time behavior of the system depends to some extent on the value of the Sutherland invariant I_s [24]. The behavior is particularly simple near $I_s = 0$ and -1 (which are respectively the maximum and minimum possible values of I_s). Near $I_s = 0$, the trajectory is given by a circle on the Bloch sphere [25]. This is similar to the behavior of SO(3) matrices discussed above, namely the point moves on an ellipse [as depicted in Fig. 2(a)] when T_0 and λ are small which corresponds to a very small value of I_s according to Eq. (A2). On increasing λ and T_0 the invariant I_s increases, resulting in an increase in the linear growth of the geodesic distance d with stroboscopic time n as shown in Fig. 2(b). For larger λ and T_0 the approximation in deriving Eq. (15) does not hold and therefore cannot explain the corresponding completely dispersed phase space as shown in Fig. 1(b). Also, the above analytical expression for the regular elliptical trajectory does not explain the precession over very long times even for small λ and T_0 shown in Fig. 1(a), which goes beyond the simple approximate calculation shown in Appendix A.

C. Quantum dynamics

We now analyze the quantum dynamics of a spin- S object governed by the time-dependent Hamiltonian in Eq. (1). To this end we construct the initial wave function $|\psi(0)\rangle$ from a spin coherent state given by [51]

$$|\Theta, \Phi\rangle = (1 + |z|^2)^{-S} e^{z\hat{S}_+} |S, -S\rangle, \quad (16)$$

where Θ and Φ are the polar and azimuthal angles, respectively, representing the orientation of the classical spin vector of magnitude S and $z = e^{-i\Phi} \tan(\Theta/2)$. The time-evolved state after the m th Fibonacci kick is given by

$$|\psi(m)\rangle = \hat{\mathcal{F}}_m |\psi(0)\rangle. \quad (17)$$

To compute the distribution of the relative phases of the time-evolved state we first construct the phase state given by [52],

$$|\varphi\rangle = \frac{1}{\sqrt{\mathcal{N}}} \sum_{l=-S}^S e^{il\varphi} |l\rangle, \quad (18)$$

where $\varphi = \varphi_0 + 2\pi l'/\mathcal{N}$ and $l' \in [1, \mathcal{N}]$, $\mathcal{N} = 2S + 1$. We choose $\varphi_0 = -\pi$ so that the relative phase lies in the range $-\pi$ to π . The phase distribution can be obtained by projecting $|\psi(m)\rangle$ onto the phase state as given by

$$p(\varphi) = |\langle\varphi|\psi(m)\rangle|^2. \quad (19)$$

In Fig. 3(a) we have shown the time evolution of $p(\varphi)$, and in Fig. 3(b) the snapshots of $p(\varphi)$ at different times are plotted. We observe the phase distribution $p(\varphi)$ remains a highly peaked function; however, its peak position changes under stroboscopic evolution. It indicates that the phase diffusion does not take place even for large kicking strengths, and the phase coherence is not lost during the time evolution. We also compute the expectation values of the spin operators, i.e., $\langle\hat{S}_z\rangle$ where the average $\langle.\rangle$ is taken with respect to the time-evolved state $|\psi(m)\rangle$. We have verified that under quantum dynamics $\langle\hat{S}_i\rangle$'s are in agreement with the classical variables S_i obtained

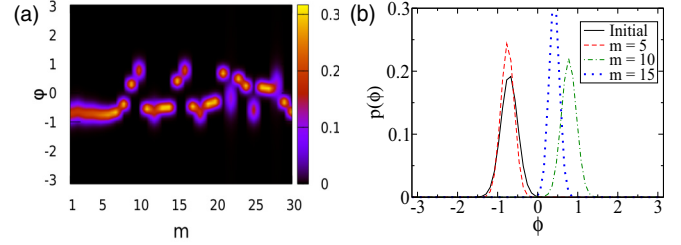


FIG. 3. (a) Time evolution of the phase distribution $p(\varphi)$ of the time-evolved state is shown in the color map where the values of $p(\varphi)$ are presented in a color scale. (b) Snapshots of the distribution $p(\varphi)$ at different Fibonacci time steps. Although the peak position of $p(\varphi)$ fluctuates, no broadening of the distribution is observed. For both figures $T_0 = \pi/100$ and $\lambda = \pi/40$.

from the dynamical map. The time evolution of the mean values of these operators exhibit fluctuations similar to the peak of $p(\varphi)$ in Fig. 3.

To understand the nature of the fluctuations in the dynamics of spin variables, we compute the cumulative sum of the Fourier transform of $\langle\hat{S}_z\rangle$ given by [31–33,36,37]

$$X_\Omega = \sum_{m=1}^N x_m e^{i2\pi\Omega m}, \quad (20)$$

where $x_m = \langle\hat{S}_z\rangle$ computed at the m th Fibonacci step and Ω is the frequency. From the power spectrum, X_Ω vs Ω , we observe that several frequency modes are present in the fluctuations which confirms that the dynamics is not at all regular even for small values of λ and T_0 for which the spin variables are seen to undergo a precessional motion in Fig. 1(a). The corresponding dynamics in the $\text{Re}[X_\Omega]$ - $\text{Im}[X_\Omega]$ plane exhibits a fractal-like structure as depicted in Fig. 4(a). The degree of such fractal motion can be quantified using the relation $|X_\Omega|^2 \sim N^\beta$, where the exponent $\beta = 1$ (2) signifies random (regular) paths, respectively, whereas $\beta \neq 1, 2$ corresponds to a fractal path in the $\text{Re}[X_\Omega]$ - $\text{Im}[X_\Omega]$ plane which can be observed from the logarithmic plot in Fig. 4(b). We have computed β for different values of Ω , i.e., $\beta(\Omega = 0.2) = 1.436$ and $\beta(\Omega = 0.4) = 1.1$, for $\lambda = \pi/50$ and $T_0 = \pi/100$ and checked that for different choices of λ and T_0 the fractal behavior remains qualitatively similar.

Next we investigate the spectral properties of the Floquet operator, $\hat{\mathcal{F}}_m$, after a sufficiently large Fibonacci step m . Due to unitarity, we have $\hat{\mathcal{F}}_m |\chi_\nu\rangle = e^{i\varepsilon_\nu} |\chi_\nu\rangle$, where $\varepsilon_\nu \in [-\pi, \pi]$ and $|\chi_\nu\rangle$ are the eigenphase and eigenvector corresponding to the ν th Floquet eigenmode. We compute the moments of the eigenstates $|\chi_\nu\rangle$ of the Floquet operator $\hat{\mathcal{F}}_m$ at the m th Fibonacci step using the relation given by

$$I_q^\nu = \sum_{m_s=-S}^S |\chi_\nu(m_s)|^{2q}, \quad I_q = \frac{1}{\mathcal{N}} \sum_\nu I_q^\nu \sim \mathcal{N}^{-\tau_q}, \quad (21)$$

where $\chi_\nu(m_s) = \langle\chi_\nu|\alpha_{m_s}\rangle$, $|\alpha_{m_s}\rangle$ being the computational basis and $\mathcal{N} = 2S + 1$ is the Hilbert space dimension of a non-interacting spin of magnitude S . The exponent τ_q is related to the fractal dimension D_q as $\tau_q = D_q(q - 1)$ [35,53–55]. The fractal dimension can equivalently be computed from

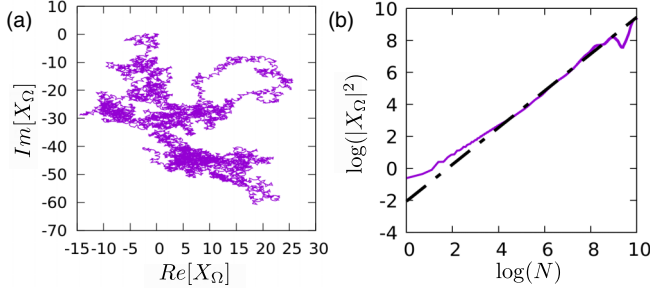


FIG. 4. (a) Stroboscopic dynamics in the $\text{Re}[X_\Omega]$ - $\text{Im}[X_\Omega]$ plane plotted at the N th Fibonacci step, where N runs from 1 to 10 000 for driving parameters $T_0 = \pi/100$, $\lambda = \pi/50$, and frequency $\Omega = 1/\beta_G$. (b) $|X_\Omega|^2$ plotted as a function of the maximum Fibonacci step N after an averaging over 10 000 realizations of the Fibonacci chain. We find that $|X_\Omega|^2 \sim N^{1.16}$.

[43,55,56]

$$D_q = \frac{S_q^v}{\log \mathcal{N}}, \quad S_q^v = - \sum_{m_s=-S}^S \frac{\log |\chi_v(m_s)|^{2q}}{(q-1)}, \quad (22)$$

where $\mathcal{N} \gg 1$ and S_q^v is the Rényi entropy corresponding to the v th eigenvector $|\chi_v\rangle$. In Figs. 5(a) and 5(b) we have plotted $\log I_q$ and the average Rényi entropy $S_q = \sum_v S_q^v / \mathcal{N}$ respectively as a function of $\log \mathcal{N}$ for different values of q . Using Eqs. (21) and (22) we obtain τ_q from the slope of the linear fitting in Figs. 5(a) and 5(b) respectively. The nontrivial behavior of τ_q with q is shown in Fig. 5(c) and hence a q -dependent fractal dimension D_q confirms the multifractality of the eigenvectors. These plots have been generated after a sufficiently large number of Fibonacci steps, say, $m \sim 30$, after which the behavior does not change with m as is evident from Fig. 5(c). We also observed that the qualitative behavior remains the same for different choices of the driving parameters λ and T_0 . It is to be noted that the scaling exponents τ_q or D_q are related to the statistical properties of the Floquet states and are extracted in the limit of large system size \mathcal{N} , which in our case turns out to be related to the spin magnitude S . Thus τ_q and D_q are computed from Eqs. (21) and (22), respectively, for a very large spin magnitude S .

Further, we explored the fractality in the eigenspectrum by counting the local number of eigenstates ΔN_ε within the interval $\Delta \varepsilon$ around the eigenphase ε . Typically in the limit $\Delta \varepsilon \rightarrow 0$, the local number of eigenstates around ε follows the relation $\Delta N_\varepsilon \sim (\Delta \varepsilon)^\alpha$, where the exponent $\alpha = 1$ is associated with band spectrum, whereas $0 < \alpha < 1$ indicates a multifractal spectrum [12,53,57,58]. In Fig. 5(d) we have shown the variation of ΔN_ε with $\Delta \varepsilon$ in a log-log plot at the center of the band ($\varepsilon \simeq 0$). From the slope of the linear fitting in Fig. 5(d) we obtain the exponent $\alpha \simeq 0.69$ which signifies fractality in the Floquet eigenspectrum. It should be noted that in general the value of α can change depending on the choice of energy ε in the band [12,53].

III. EFFECTS OF INTERACTIONS

In this section we study the effects of interactions by considering a system of two interacting spins each of magnitude

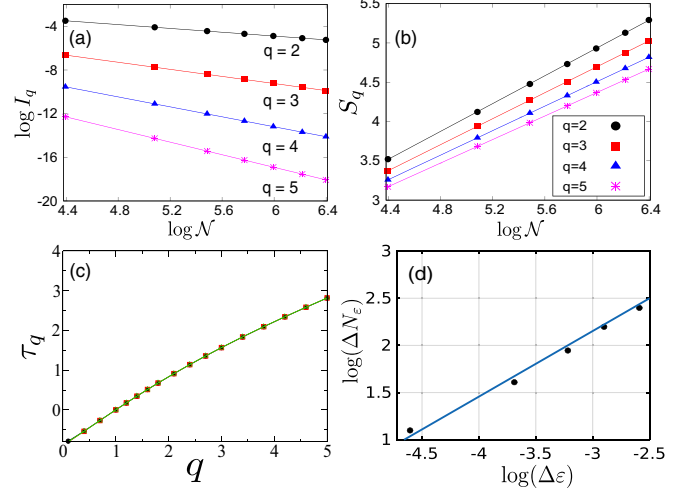


FIG. 5. Multifractality of Floquet states: Log-log plot of variation of (a) moments I_q and (b) Shannon entropy S_q of Floquet states with Hilbert space dimension \mathcal{N} . (c) τ_q vs q , extracted from (a) and (b) using Eqs. (21) and (22) respectively, for a typical choice of parameters $\lambda = \pi/10$ and $T_0 = \pi/10$. Note that the graphs calculated for different Fibonacci steps m overlap with each other for sufficiently large m . (d) Multifractal Floquet eigenspectrum: Log-log plot of number of states ΔN_ε vs $\Delta \varepsilon$ computed at the band center ($\varepsilon \simeq 0$). The exponent $\alpha \simeq 0.69$ is extracted from the slope of linear fitting of the numerical data points (dots). The parameters used are $T_0 = \pi/100$, $\lambda = \pi/50$, and $\mathcal{N} = 801$ ($S = 400$).

S , and a δ -function kick is applied to both the spins following a Fibonacci sequence. Our goal is to study (i) the fate of the multifractality of the Floquet states and the spectrum of the evolution operator in the presence of interactions and (ii) the validity of the semiclassical dynamics in terms of coherent states for large spins and whether the interactions can lead to thermalization.

The Hamiltonian describing such quasiperiodically driven interacting system is given by

$$\hat{H}(t) = \hat{H}_0 + \lambda \hat{S}_x^{A/B} \sum_{n=-\infty}^{\infty} \delta\left(t - \sum_n T_n\right),$$

$$\hat{H}_0 = \hat{S}_z^A + \hat{S}_z^B - J \hat{S}_z^A \hat{S}_z^B. \quad (23)$$

This is a simple generalization of the noninteracting model discussed above, where J is the strength of the interaction between the two spins, and the last term represents kicks applied to the two spins following a Fibonacci sequence. The Floquet operators for the first two Fibonacci step are therefore given by

$$\hat{\mathcal{F}}_1^I = e^{-iT\hat{H}_0} e^{-i\lambda\hat{S}_x^A}, \quad \hat{\mathcal{F}}_2^I = e^{-iT\hat{H}_0} e^{-i\lambda\hat{S}_x^B}. \quad (24)$$

The subsequent matrices in the Fibonacci sequence are then generated using Eq. (7). By diagonalizing the Floquet matrix $\hat{\mathcal{F}}_m^I$ we obtain the eigenphases ε_v and the corresponding eigenvectors $|\chi_v\rangle$ (see Sec. II C). We first compute the spacing between the successive eigenphases, i.e., $\delta_v = \varepsilon_{v+1} - \varepsilon_v$, and calculate the distribution of the δ_v 's following the procedure described in Ref. [59] in order to keep the normalization $\int P(\delta)d\delta = 1$ and mean $\int \delta P(\delta)d\delta = 1$. In Figs. 6(a)

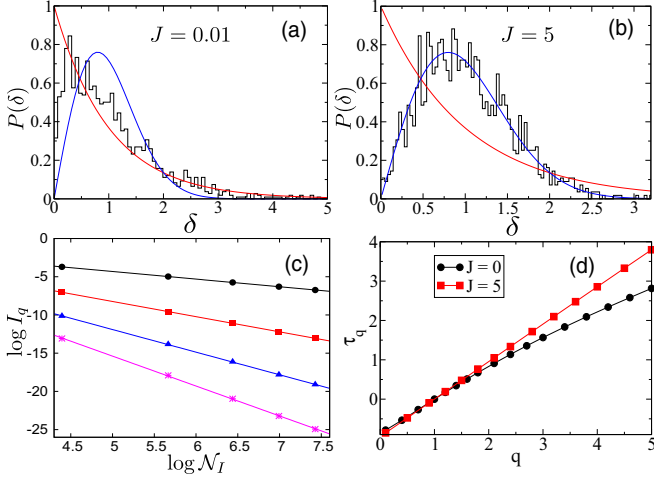


FIG. 6. [(a) and (b)] Distribution $P(\delta)$ of the spacing between eigenphases δ for $J = 0.01$ and $J = 5$, respectively, for $S = 20$ ($\mathcal{N}_I = 1681$) and computed at Fibonacci step $n = 50$. (c) $\log I_q$ vs $\log \mathcal{N}_I$ and (d) τ_q vs q for $J = 5$. The behavior of the corresponding noninteracting system ($J = 0$) is shown by the black circles. Here and in the rest of the figures we set $T = \pi/100$ and $\lambda = \pi/10$.

and 6(b) we have plotted the normalized quasienergy spacing distribution $P(\delta)$ for small and large values of J , respectively. We note that in the presence of interactions, the fractality of the system vanishes and level repulsion sets in. For large J , $P(\delta)$ resembles the Wigner surmise and corresponds to the Gaussian orthogonal ensemble of random matrix theory as shown in Fig. 6(b); this indicates a possible thermalization of the system for large values of the interaction strength J [60].

We compute the moments of the Floquet eigenstates using Eq. (21) followed by a calculation of the exponent τ_q which is related to the fractal dimension D_q . In Fig. 6(c) we have plotted $\log I_q$ vs $\log \mathcal{N}_I$ for different values of q , where $\mathcal{N}_I = (2S + 1)^2$ is the Hilbert space dimension. From the linear fitting we obtain the slope τ_q which we have plotted in Fig. 6(d) as a function of q and compared with the case $J = 0$. We note that in contrast to the noninteracting case, we find for finite values of the interaction strength J that $\tau_q \sim q$; this implies $D_q \sim 1$ indicating an ergodic nature of the Floquet eigenstates.

We further elucidate this fact from the wave packet dynamics. We construct an initial wave function from the product of two spin coherent states given by

$$|\psi_{AB}(0)\rangle = |\Theta, \Phi\rangle_A \otimes |\Theta, \Phi\rangle_B. \quad (25)$$

The dynamics of the expectation values of the corresponding spin observables are illustrated in Appendix B. From the time-evolved wave function, $|\psi_{AB}(m)\rangle = \hat{F}_m^I |\psi_{AB}(0)\rangle$, we compute the reduced density matrix corresponding to either of the spins A and B using the relation,

$$\hat{\rho}_{A(B)}^m = \text{Tr}_{B(A)} |\psi_{AB}(m)\rangle \langle \psi_{AB}(m)|, \quad (26)$$

where $\text{Tr}(\cdot)$ represents partial tracing with respect to spin B or A. In Fig. 7 we have shown the structure of $\hat{\rho}_A^m$ after Fibonacci step $m = 50$ which, we have checked, is sufficient to obtain the steady states. For small values of J , $\hat{\rho}_A^m$ contains both the diagonal and off-diagonal entries in the eigenbasis

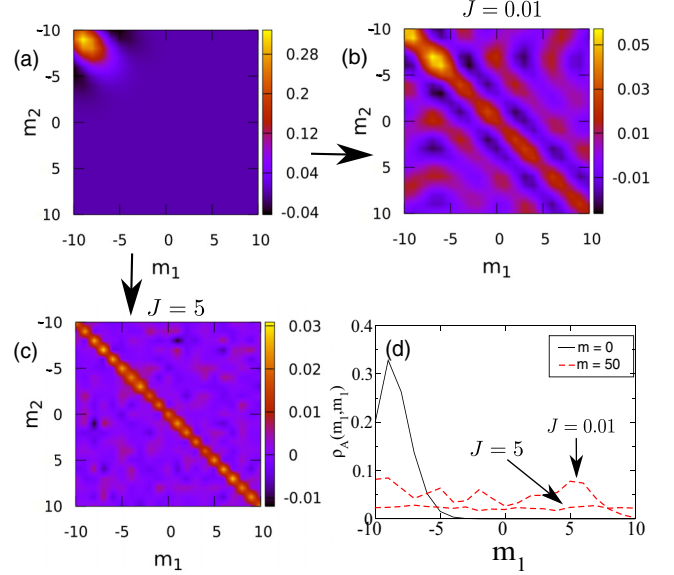


FIG. 7. [(a)–(c)] Time evolution of the subsystem reduced density matrix $\hat{\rho}_A$ for $J = 0.01$ and $J = 5$, respectively, for $S = 10$. (d) Plots of the corresponding diagonal elements.

of \hat{S}_z indexed by m_1, m_2 which can be observed in Fig. 7 (b). On the other hand, for large values of J , $\hat{\rho}_A^m$ becomes completely diagonal as is evident from Fig. 7(c), with equally weighted entries, i.e., $\rho_A^m(m_1, m_1) \sim 1/\mathcal{N}$. Such an observation indicates that in the presence of interactions the coherent state picture is lost and leads us to conclude that the system approaches a diagonal ensemble and thermalizes to infinite temperature [60–63].

IV. CONCLUSIONS

To summarize, we have studied the dynamics of a spin- S object which has a well-defined classical limit and is subjected to quasiperiodic kicks following the Fibonacci sequence. By evolving the corresponding classical Hamiltonian map of the spin variables we obtained the phase portraits which, for small kicking strength λ and time period T_0 , exhibits regular orbits which precess over an unit sphere. Interestingly, for increasing λ and T_0 the dynamics appears to be chaotic; however, the Lyapunov exponent vanishes. We have calculated the Sutherland invariant which constrains to some extent the dynamics governed by the transfer matrix with $\text{SO}(3)$ symmetry. Fluctuations of the classical counterpart of the spin dynamics exhibit a fractal structure which is verified by its Fourier spectrum analysis. It turns out that for an initially chosen spin coherent state, the phase coherence is retained during the time evolution under Fibonacci drive even for large λ and T_0 indicating classical-quantum correspondence. Fractality in classical dynamics is observed from the spectral analysis. More interestingly, the fractality is also present in the internal structure of the Floquet matrix governing the full quantum dynamics which has been investigated from the scaling of the Rényi entropy, as well as from the moments of the Floquet eigenvectors and the quasienergy spectrum. Finally, we have considered two such spin- S objects interacting with each

other and driven quasiperiodically. We have shown that in the presence of the interaction, the fractal behavior vanishes and level repulsion sets in the Floquet quasienergy spectrum. In the dynamics, we observed that for increasing interaction strength J , the average values of the components of spin operators for both the spins saturate to zero and the reduced density matrix for either of the spins becomes diagonal. The emergence of the diagonal ensemble with equally weighted diagonal elements indicates thermalization of the system to infinite temperature and corresponds to the microcanonical ensemble of statistical mechanics.

In conclusion, a quasiperiodically driven large spin system is a simple but fascinating model with multifractal Floquet eigenstates and eigenspectrum, and at the same time its dynamics in the classical limit corresponds to strange nonchaotic attractors. Moreover it exhibits a nonergodic to ergodic transition in the presence of interactions. Kicked spin models have already been realized in experiments considering the angular momentum of an atom in a suitable hyperfine state [64,65]; the kicks can be generated by using a short magnetic pulse [66]. The dynamics of such kicked systems can also be investigated in circuit QED experiments [67]. The signature of fractality and its change to ergodic behavior in the dynamics can be found in the experiments by measuring the discrete time Fourier amplitude spectrum of time varying physical observable such as the spin variables in our study as well from the dimension measurement [34]. The models discussed in our paper can thus be realized and therefore our results can be tested in the similar experiments.

ACKNOWLEDGMENTS

S.R. thanks Anandamohan Ghosh for useful discussions. D.S. thanks Department of Science and Technology (DST), India, Project No. SR/S2/JCB-44/2010 for financial support. S.R. acknowledges the financial support and hospitality provided by Indian Institute of Science Education and Research - Kolkata (IISER Kolkata), India for this work.

APPENDIX A: SUTHERLAND INVARIANT FOR SO(3) MATRICES

We consider the transfer matrix J_n , given in Eq. (5) which is a SO(3) matrix. Starting with two such matrices J_1 and J_2

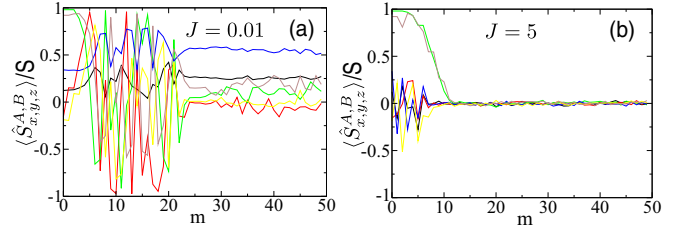


FIG. 8. [(a) and (b)] Time evolution of $\langle \hat{S}_{x,y,z}^{A,B} \rangle$ for $J = 0.01$ and $J = 5$, respectively, for $S = 10$.

given by

$$J_1 = e^{-i\lambda T_x} \quad \text{and} \quad J_2 = e^{-i2T_0 T_z} e^{-i\lambda T_x}, \quad (\text{A1})$$

we find that the corresponding Sutherland invariant is

$$I_s = -[\sin T_0 \sin(\lambda/2)]^2. \quad (\text{A2})$$

We have checked numerically up to a large Fibonacci step $m \sim 1000$ that I_s remains constant during the time evolution.

It is known that the m th Fibonacci number, given by $F_m = [\beta_G^m - (-1)^m / \beta_G] / \sqrt{5}$, quickly approaches the value $\beta_G^m / \sqrt{5}$ as m increases. We then find that

$$J_m = e^{-i\beta_G^m [\lambda T_x + (2T_0/\beta_G) T_z] / \sqrt{5}}, \quad (\text{A3})$$

which has been derived under the approximation that $\lambda, T_0 \ll 1$ so that the commutators arising from $[T_i, T_j]$ do not grow much within a small timescale. This leads us to define

$$\phi_m = -\frac{\beta_G^m}{\sqrt{5}} \bar{\lambda} \quad \text{and} \quad \hat{e}_m = \frac{1}{\bar{\lambda}} (\lambda, 0, 2T_0/\beta_G), \quad (\text{A4})$$

where $\bar{\lambda} = \sqrt{\lambda^2 + 4T_0^2/\beta_G^2}$.

APPENDIX B: DYNAMICS OF SPIN OBSERVABLES IN THE PRESENCE OF INTERACTION

To study the dynamics of the spin variables, we compute the expectation values of the spin operators, i.e., $\langle \hat{S}_{x,y,z}^{A,B} \rangle$, where $\langle \cdot \rangle$ is taken from the time-evolved wave function $|\psi_{AB}(m)\rangle = \hat{\mathcal{F}}_m^I |\psi_{AB}(0)\rangle$.

We observe that for small values of the interaction strength J , $\langle \hat{S}_{x,y,z}^{A,B} \rangle$ saturates to different nonzero values, whereas for large J , all the spin observables decays to zero as depicted in Figs. 8(a) and 8(b), respectively.

-
- [1] D. Shechtman, I. Blech, D. Gratias, and J. W. Cahn, *Phys. Rev. Lett.* **53**, 1951 (1984).
- [2] P. J. Steinhardt and S. Ostlund, *The Physics of Quasicrystals* (World Scientific, Singapore, 1987).
- [3] A. I. Goldman and R. F. Kelton, *Rev. Mod. Phys.* **65**, 213 (1993).
- [4] R. Lifshitz, *Rev. Mod. Phys.* **69**, 1181 (1997).
- [5] M. Quilichini, *Rev. Mod. Phys.* **69**, 277 (1997).
- [6] G. Roati, C. D'Errico, L. Fallani, M. Fattori, C. Fort, M. Zaccanti, G. Modugno, M. Modugno, and M. Inguscio, *Nature (London)* **453**, 895 (2008).
- [7] C. Aulbach, A. Wobst, G. L. Ingold, P. Hänggi, and I. Varga, *New J. Phys.* **6**, 70 (2004); M. Modugno, *ibid.* **11**, 033023 (2009).
- [8] S. Iyer, V. Oganessian, G. Refael, and D. A. Huse, *Phys. Rev. B* **87**, 134202 (2013).
- [9] M. Schreiber, S. S. Hodgman, P. Bordia, H. P. Lüschen, M. H. Fischer, R. Vosk, E. Altman, U. Schneider, and I. Bloch, *Science* **349**, 842 (2015).
- [10] P. Bordia, H. P. Lüschen, S. S. Hodgman, M. Schreiber, I. Bloch, and U. Schneider, *Phys. Rev. Lett.* **116**, 140401 (2016).

- [11] F. Piéchon, *Phys. Rev. Lett.* **76**, 4372 (1996); S. Abe and H. Hiramoto, *Phys. Rev. A* **36**, 5349 (1987).
- [12] M. Kohmoto, *Phys. Rev. Lett.* **51**, 1198 (1983); C. Tang and M. Kohmoto, *Phys. Rev. B* **34**, 2041 (1986); M. Kohmoto, B. Sutherland, and C. Tang, *ibid.* **35**, 1020 (1987).
- [13] X. Deng, S. Ray, S. Sinha, G. V. Shlyapnikov, and L. Santos, *Phys. Rev. Lett.* **123**, 025301 (2019); A. Szabó and U. Schneider, *Phys. Rev. B* **98**, 134201 (2018).
- [14] V. K. Varma, C. de Mulatier, and M. Žnidarič, *Phys. Rev. E* **96**, 032130 (2017).
- [15] P. J. D. Crowley, I. Martin, and A. Chandran, *Phys. Rev. B* **99**, 064306 (2019).
- [16] S. Aubry and G. André, *Ann. Isr. Phys. Soc.* **3**, 133 (1980).
- [17] Y. Lahini, R. Pugatch, F. Pozzi, M. Sorel, R. Morandotti, N. Davidson, and Y. Silberberg, *Phys. Rev. Lett.* **103**, 013901 (2009).
- [18] R. Nandkishore and D. A. Huse, *Annu. Rev. Condens. Matter Phys.* **6**, 15 (2015); E. Altman and R. Vosk, *ibid.* **6**, 383 (2015).
- [19] D. A. Abanin, E. Altman, I. Bloch, and M. Serbyn, *Rev. Mod. Phys.* **91**, 021001 (2019).
- [20] P. Bordia, H. Lüschen, U. Schneider, M. Knap, and I. Bloch, *Nat. Phys.* **13**, 460 (2017).
- [21] P. Ponte, A. Chandran, Z. Papić, and D. A. Abanin, *Ann. Phys.* **353**, 196 (2015); P. Ponte, Z. Papić, F. Huveneers, and D. A. Abanin, *Phys. Rev. Lett.* **114**, 140401 (2015).
- [22] L. D'Alessio, Y. Kafri, A. Polkovnikov, and M. Rigol, *Adv. Phys.* **65**, 239 (2016).
- [23] S. Ray, A. Ghosh, and S. Sinha, *Phys. Rev. E* **97**, 010101(R) (2018); S. Ray, S. Sinha, and K. Sengupta, *Phys. Rev. A* **98**, 053631 (2018).
- [24] S. Nandy, A. Sen, and D. Sen, *Phys. Rev. B* **98**, 245144 (2018).
- [25] S. Maity, U. Bhattacharya, A. Dutta, and D. Sen, *Phys. Rev. B* **99**, 020306(R) (2019).
- [26] S. Ostlund, R. Pandit, D. Rand, H. J. Schellnhuber, and E. D. Siggia, *Phys. Rev. Lett.* **50**, 1873 (1983).
- [27] M. Kohmoto, L. P. Kadanoff, and C. Tang, *Phys. Rev. Lett.* **50**, 1870 (1983).
- [28] B. Sutherland, *Phys. Rev. Lett.* **57**, 770 (1986).
- [29] K. Singh, K. Saha, S. A. Parameswaran, and D. M. Weld, *Phys. Rev. A* **92**, 063426 (2015); B. Pal and K. Saha, *Phys. Rev. B* **97**, 195101 (2018).
- [30] D. Ruelle and F. Takens, *Commun. Math. Phys.* **20**, 167 (1971); C. Grebogi, E. Ott, S. Pelikan, and J. A. Yorke, *Physica D (Amsterdam)* **13**, 261 (1984).
- [31] A. S. Pikovsky and U. Feudel, *J. Phys. A* **27**, 5209 (1994).
- [32] T. Yalcinkaya and Y. C. Lai, *Phys. Rev. E* **56**, 1623 (1997).
- [33] M. Agrawal, A. Prasad, and R. Ramaswamy, *Phys. Rev. E* **81**, 026202 (2010).
- [34] W. L. Ditto, M. L. Spano, H. T. Savage, S. N. Rauseo, J. Heagy, and E. Ott, *Phys. Rev. Lett.* **65**, 533 (1990).
- [35] I. Guarneri and M. D. Meo, *J. Phys. A* **28**, 2717 (1995).
- [36] J. M. Luck, H. Orland, and U. Smilansky, *J. Stat. Phys.* **53**, 551 (1988).
- [37] P. M. Blekher, H. R. Jauslin, and J. L. Lebowitz, *J. Stat. Phys.* **68**, 271 (1992).
- [38] T. Geisel, *Phys. Rev. A* **41**, 2989 (1990).
- [39] P. T. Dumitrescu, R. Vasseur, and A. C. Potter, *Phys. Rev. Lett.* **120**, 070602 (2018).
- [40] E. Altman, *Nat. Phys.* **14**, 979 (2018); D. J. Luitz and Y. Bar Lev, *Phys. Rev. Lett.* **117**, 170404 (2016); E. J. Torres-Herrera and L. F. Santos, *Phys. Rev. B* **92**, 014208 (2015); M. Serbyn, Z. Papić, and D. A. Abanin, *ibid.* **96**, 104201 (2017).
- [41] B. L. Altshuler, E. Cuevas, L. B. Ioffe, and V. E. Kravtsov, *Phys. Rev. Lett.* **117**, 156601 (2016); M. Pino, L. B. Ioffe, and B. L. Altshuler, *Proc. Natl. Acad. Sci. USA* **113**, 536 (2016); A. De Luca, B. L. Altshuler, V. E. Kravtsov, and A. Scardicchio, *Phys. Rev. Lett.* **113**, 046806 (2014).
- [42] C. Monthus, *J. Stat. Mech.* (2016) 073301; T. Micklitz, F. Monteiro, and A. Altland, *Phys. Rev. Lett.* **123**, 125701 (2019).
- [43] Y. Y. Atas and E. Bogomolny, *Phys. Rev. E* **86**, 021104 (2012); *Philos. Trans. R. Soc. Lond. A* **372**, 20120520 (2014).
- [44] J. Lindinger, A. Buchleitner, and A. Rodríguez, *Phys. Rev. Lett.* **122**, 106603 (2019).
- [45] J.-M. Stéphan, G. Misguich, and V. Pasquier, *Phys. Rev. B* **84**, 195128 (2011).
- [46] A. Richardella, P. Roushan, S. Mack, B. Zhou, D. A. Huse, D. D. Awschalom, and A. Yazdani, *Science* **327**, 665 (2010).
- [47] Here we call the time evolution operator between two consecutive kicks the Floquet operator.
- [48] R. Blümel, *Phys. Rev. Lett.* **73**, 428 (1994).
- [49] R. Schack, *Phys. Rev. Lett.* **75**, 581 (1995).
- [50] A. S. Pikovsky, M. A. Zaks, and J. Kurths, *J. Phys. A* **29**, 295 (1996).
- [51] J. M. Radcliffe, *J. Phys. A* **4**, 313 (1971).
- [52] R. Gati and M. K. Oberthaler, *J. Phys. B* **40**, 61 (2007).
- [53] J. X. Zhong and T. Geisel, *Phys. Rev. E* **59**, 4071 (1999).
- [54] S. Roy, I. M. Khaymovich, A. Das, and R. Moessner, *SciPost Phys.* **4**, 025 (2018).
- [55] E. J. Torres-Herrera and L. F. Santos, *Ann. Phys. (Berlin)* **529**, 1600284 (2017).
- [56] X. Chen, B. Hsu, T. L. Hughes, and E. Fradkin, *Phys. Rev. B* **86**, 134201 (2012).
- [57] R. Ketzmerick, K. Kruse, and T. Geisel, *Phys. Rev. Lett.* **80**, 137 (1998).
- [58] S. Ostlund and R. Pandit, *Phys. Rev. B* **29**, 1394 (1984).
- [59] F. Haake, *Quantum Signatures of Chaos*, Springer Series in Synergetics, Vol. 54 (Springer, Berlin, 2010).
- [60] S. Ray, A. Ghosh, and S. Sinha, *Phys. Rev. E* **94**, 032103 (2016).
- [61] A. Russomanno, R. Fazio, and G. E. Santoro, *Europhys. Lett.* **110**, 37005 (2015).
- [62] N. Regnault and R. Nandkishore, *Phys. Rev. B* **93**, 104203 (2016).
- [63] L. D'Alessio and M. Rigol, *Phys. Rev. X* **4**, 041048 (2014).
- [64] G. A. Smith, A. Silberfarb, I. H. Deutsch, and P. S. Jessen, *Phys. Rev. Lett.* **97**, 180403 (2006).
- [65] S. Chaudhury, S. Merkel, T. Herr, A. Silberfarb, I. H. Deutsch, and P. S. Jessen, *Phys. Rev. Lett.* **99**, 163002 (2007).
- [66] S. Chaudhury, A. Smith, B. E. Anderson, S. Ghose, and P. S. Jessen, *Nature (London)* **461**, 768 (2009).
- [67] C. Neill, P. Roushan, M. Fang, Y. Chen, M. Kolodrubetz, Z. Chen, A. Megrant, R. Barends, B. Campbell, B. Chiaro, A. Dunsworth, E. Jeffrey, J. Kelly, J. Mutus, P. J. J. O'Malley, C. Quintana, D. Sank, A. Vainsencher, J. Wenner, T. C. White, A. Polkovnikov, and J. M. Martinis, *Nat. Phys.* **12**, 1037 (2016).